Mechanics & Industry **17**, 202 (2016)

DOI: 10.1051/meca/2015069
www.mechanics-industry.org

Mechanics & Industry

Numerical investigation of oil-water drainage and imbibition in digitized sandstones

X. Nie[a], V. Gundepalli, Y. Mu, R. Sungkorn and J. Toelke

Ingrain Inc. Houston, TX 77027, USA

Received 26 January 2015, Accepted 21 July 2015

Abstract – We simulated the primary drainage and first imbibition processes in a numerical porous-plate experiment using a lattice-Boltzmann based pore scale simulator. The pore space representations of the Berea, Fontainebleau and Bentheimer sandstones were obtained by high resolution micro-CT and subsequent segmentation. The pore body and throat distributions were identified using an open-map based method. The rock surface was assumed completely water wet. The capillary pressure as function of water saturation and the oil and water distributions were investigated for different geometries represented by the different sandstone samples. The calculated residual oil saturation after imbibition compares well with recently published high quality laboratory data. The dependence of the residual oil saturation on the initial oil saturation was calculated and the results are consistent with published experimental data and correlations. Finally the drainage and imbibition processes were calculated for several Fontainebleau samples with different porosity. It was found that the residual oil saturation decreases with porosity and the variation agrees well with published experimental data.

Key words: Digitized rock / oil and water / drainage and imbibition / sandstone / lattice Boltzmann

1 Introduction

Oil-water drainage and imbibition processes in rocks are of fundamental interest to oil industry. For long time, the applied capillary pressure at different water saturations was measured experimentally [1–5]. Due to the emergence of advanced computerized tomography (CT) technology, high-performance computing and advanced computational methods, the numerical study of drainage and imbibition has become feasible. The rock geometry can be digitized into a 3D voxel matrix representing solids and pores. In order to calculate the transport of multiphase flow, either pore network model (PNM) or direct numerical simulation (DNS) can be used. PNM replaces real pore bodies and throat shapes with geometric shapes such as ducts with circular, rectangular and triangular or more complex cross sections [6, 7]. The fluid transport and distribution are determined by employing analytical or semi-analytical solutions for the individual elements that are coupled together. DNS directly simulates two phase flow including two phase interaction characterized by interface tension and flow-wall interaction represented by contact angle in complicated rock surfaces. We use a DNS method, the lattice-Boltzmann method (LBM) which directly simulates the fundamental equations of multiphase flow in the pore space using simplified kinetic equations [8–12]. The LBM has emerged as an alternative numerical technique for simulating fluid flow for three decades. It can simulate the fluid equations accurately and efficiently, and still preserve some of the advantages of kinetic equations, such as being very suitable for parallel processing and accurately simulating flows with complicated wall geometries and interfaces. This study employs a LBM method to investigate the oil-water drainage and imbibition process in three kinds of sandstone rocks samples and effects of the geometry, initial oil situation and porosity on the results. We digitized a total of 10 rock samples including one Berea, one Bentheimer and eight Fontainebleau using micro-CT. The pore body and throat size distributions were identified using an open-map based approach [13, 14]. We discuss the features of the PC curves, the water and oil distributions and specially the residual oil saturation (S_{or}) after imbibition.

[a] Corresponding author: xiaobo@ingrainrocks.com

Table 1. Rock samples used in the simulation and digital properties. Here Δx is the voxel length, L is the dimension of rock sample, ϕ is the porosity, K_a is the absolute permeability and FF is the formation factor.

Rock Type	Δx (μm)	L (Δx)	φ	K_a (md)	FF
Berea	2.2	600^3	0.192	1221	19
Bentheimer	2.46	550^3	0.220	3048	14
Fontainebleau1	1.87	550^3	0.114	270	50.5
Fontainebleau2	2.23	500^3	0.0633	20.6	286
Fontainebleau3	2.3	500^3	0.0719	50.7	199
Fontainebleau4	2.2	500^3	0.0904	122	109
Fontainebleau5	2.34	500^3	0.150	826	27.4
Fontainebleau6	3.0	$320 \times 320 \times 486$	0.155	584	32.1
Fontainebleau7	2.3	500^3	0.221	2949	12.3
Fontainebleau8	2.38	500^3	0.228	3802	11.7

2 Material and simulation methods

As listed in Table 1, 10 sand stone samples are considered. We used the first 3 samples, Berea, Bentheimer and Fontainebleau1 to investigate the dependence of S_{or} on rock geometry. In order to compare with recently published experimental data [1], we selected samples which have similar porosity, permeability and formation factor as those used in the experiment. The samples Fontainebleau 1-8 (FB 1-8) have different porosity and were used to investigate the variation of S_{or} with porosity.

Figure 1 shows 3D pore structures and 2D slices of the Berea, Bentheimer and FB1. Their pore body shapes look different. We used a morphological approach [13] to compute pore body size distributions and a digital mercury injection experiment to compute pore throat distributions [14]. As shown in Figure 2, the pore body radius distributions have small differences while the three rock samples have obviously different pore throat size distributions. The Bentheimer sample has the largest throat size and the FB1 has the smallest. The average throat sizes of the Berea, Bentheimer and Fontainebleau samples are 9.6, 12 and 7.7 μm.

A LBM solver has been developed to simulate multiphase flow in the imbibition and drainage processes. The LBM solver uses a D3Q13 multiphase model that has multiple relaxation times [15]. The solver was parallelized for multiple CPUs and GPUs using MPI and CUDA. To cope with the large computational demand the simulations were run on high performance computing hardware. In the LBM the fluid wall interaction is modeled by wall wettability and fluid density fraction. The contact angle can be set by assigning certain wettability to the wall surface. A water wet surface may change to less water wet or even oil wet when oil stays in contact with that surface long enough, such as the surfaces of pores occupied by oil in a reservoir or the oil-aged rock surfaces in experiments. In our LBM simulations only the intrinsic contact angle is assigned if the wall roughness is resolved. The receding and advancing contact angles are determined by the wall wettability and roughness through the fluid-wall interaction. If the wall roughness is not resolved, receding and advancing contact angles are input parameters. In pore network modeling, the receding and advancing contact angles are always input parameters. In this study the wettability was assumed to be strongly water wet to compare to the water-wet experiments. We developed special boundary conditions at the solid wall to model thin water- or oil-film flows that allow transport of fluids through those thin films. The water film appears on the water wet solid surface and the oil film on the oil wet surface. We simulated a digital porous plate experiment as described in reference [12]. In the digital porous plate experiment, the one surface of the rock is attached to an oil reservoir and the opposite surface is attached to a water reservoir. If a water film is connected to the water reservoir through bulk water or a water film, the pressure boundary condition is applied to the water that contacts with the film. Otherwise the bounce back boundary condition is applied to the water solid surface. A similar boundary condition is applied to the oil. These boundary conditions prevent e.g.: unrealistic high values of trapped water in the drainage and allow snap-off effects through the films in imbibition. In the digital porous plate experiment, the water pressure is kept constant throughout the simulation. In the drainage process the oil pressure increases step by step till the desired residual water saturation is reached. In the imbibition process the oil pressure decreases till it reaches the water pressure (only controlled spontaneous imbibition). The pressure difference between oil and water is called the applied capillary pressure.

3 Results and discussions

The drainage and imbibition processes were calculated for the samples listed in Table 2. A zero contact angle was assigned to the water. The interfacial tension was set to 0.03 N.m^{-1}. In Figure 3 the applied capillary pressure for three different rock samples is shown as function of water saturation. The water saturation at the end of drainage in the simulation was matched with the experimental data in reference [1]. The petrophysical properties of rock sample and the calculated residual oil saturation for the experiments and the LBM simulations are listed in Table 2.

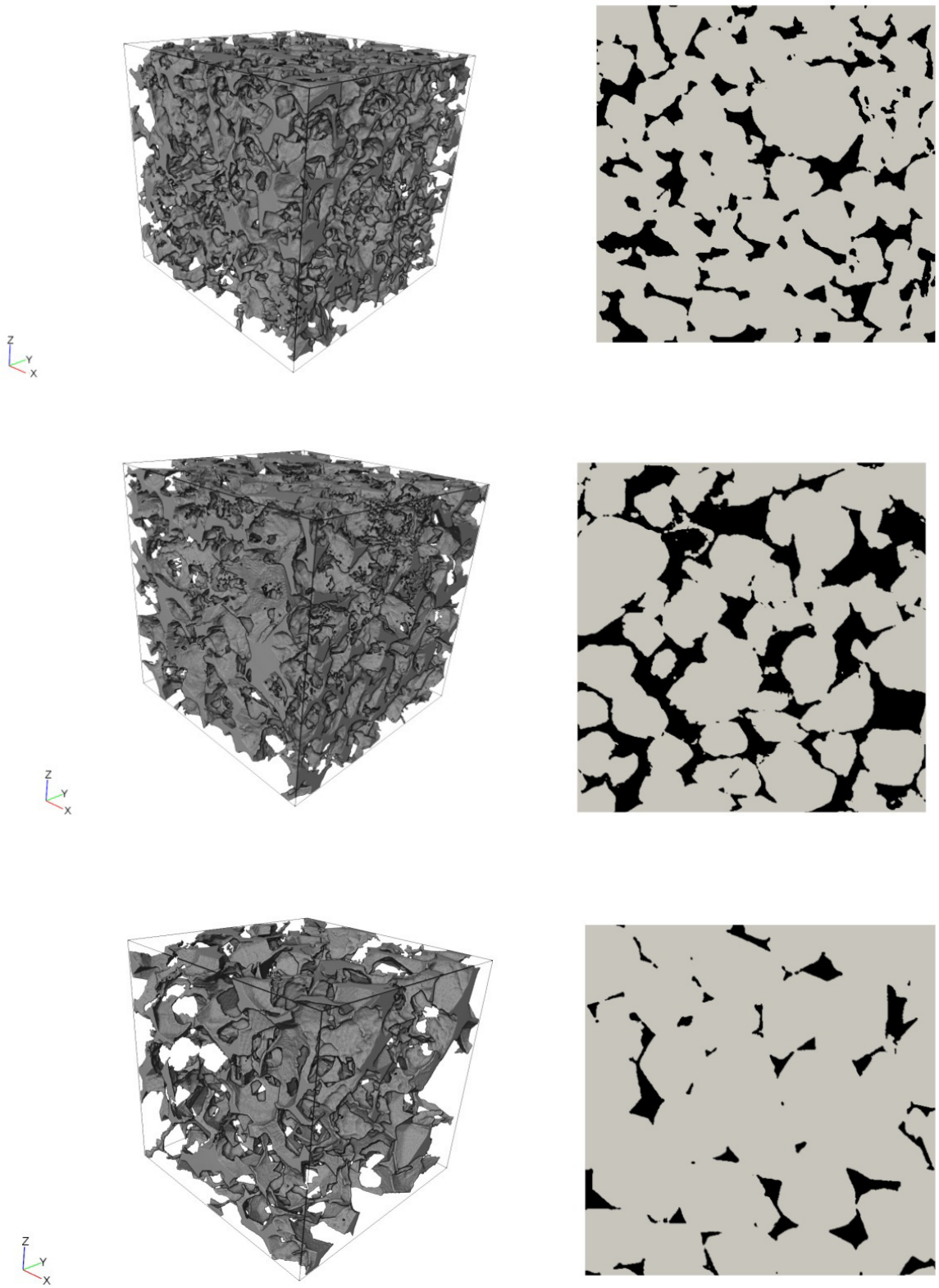

Fig. 1. 3D pore structures and 2D slices of Berea, Bentheimer and Fontainebleau samples. Pore space is black in 2D slices.

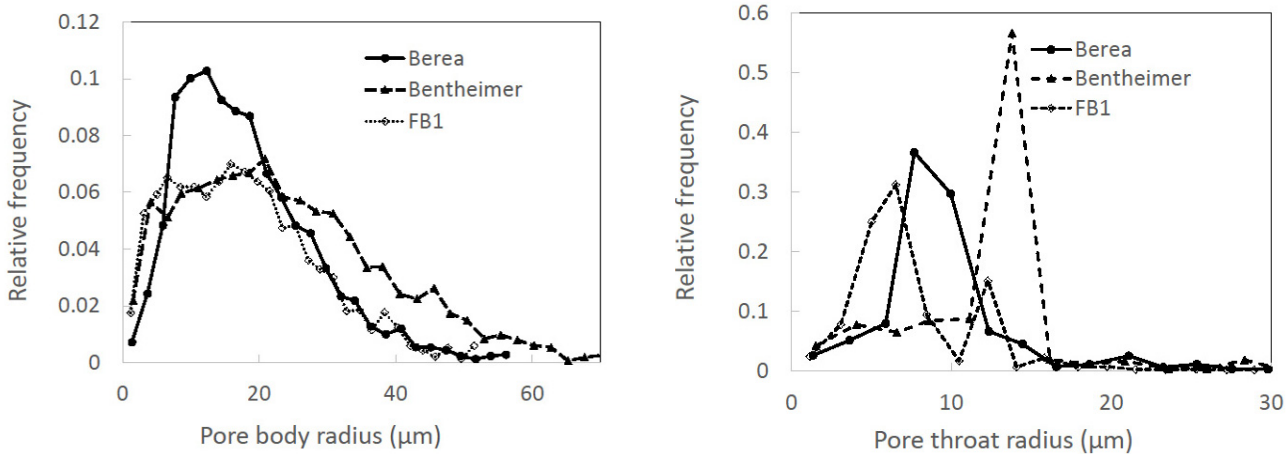

Fig. 2. Pore body (left) and pore throat (right) radii distributions for Berea, Bentheimer and Fontainebleau samples.

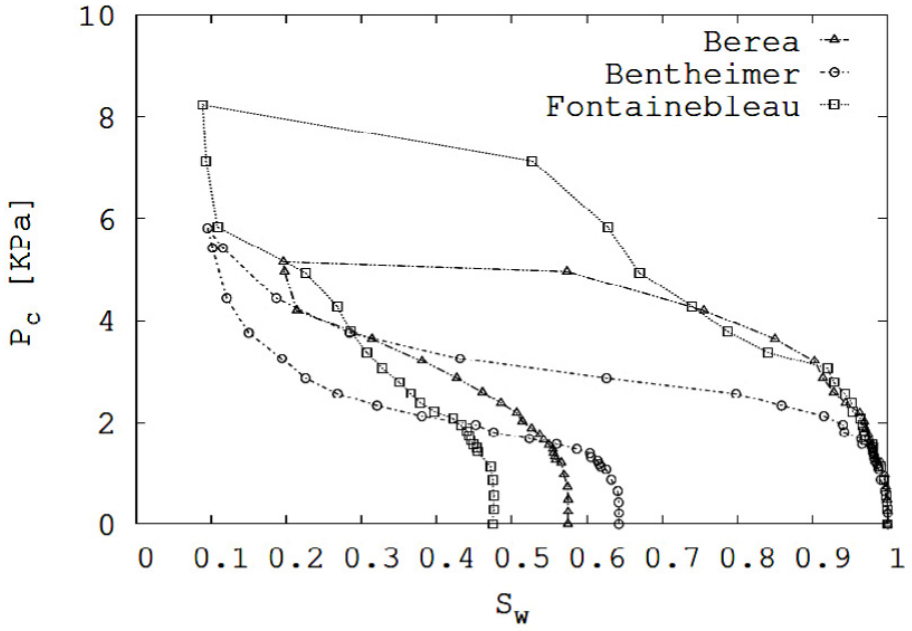

Fig. 3. Applied capillary pressure as function of water saturation for Berea, Bentheimer and Fontainebleau sandstones.

Reference [1] reports two sets of results for plugs that were about 8 cm in length and 3.3 cm in diameter and min-plugs that were 6 mm in length and 5.9 mm in diameter. Our results for Berea and Bentheimer are close to the experiment results. The simulation result of Fontainebleau is much larger than the experimental one. However it was found that the simulation result is consistent with more systematic experimental results reported in reference [5] as shown in Figure 11. The experiment results of S_{or} at the porosity of Fontainebleau 1 (0.114) spread from 0.52 to 0.62 and the simulation result is 0.525. It was pointed out in reference [5] that the observed smaller value of S_{or} for Fontainebleau rocks in experiments might result from gas diffusion. Since the contact angle was the same in the simulations, the difference of S_{or} resulted from different geometries characterized by the pore structure of the rocks. It is noticed that the residual oil saturation correlates proportionally with the ratio of pore body to pore throat size ratio of the rock samples shown in Figure 2.

Figure 4 shows the 3D structures of residual oil and 2D slices of oil and water distributions after imbibition for the three rock samples. The oil is trapped in the center of the pore because the rock surface is water wet. The water stays in pore throats and on solid surfaces. The shape of small oil cluster is sphere-like and the large clusters occupy several pore bodies resembling the pore structure of the rock which is consistent with the reported experimental results in reference [16].

In the drainage and imbibition processes the mean pressure gradient is applied along z direction. It is found that the trapped oil is uniform along the other two transverse directions and the trapped oil fraction increases with z coordinate. The less oil presents near the end at $z = 0$

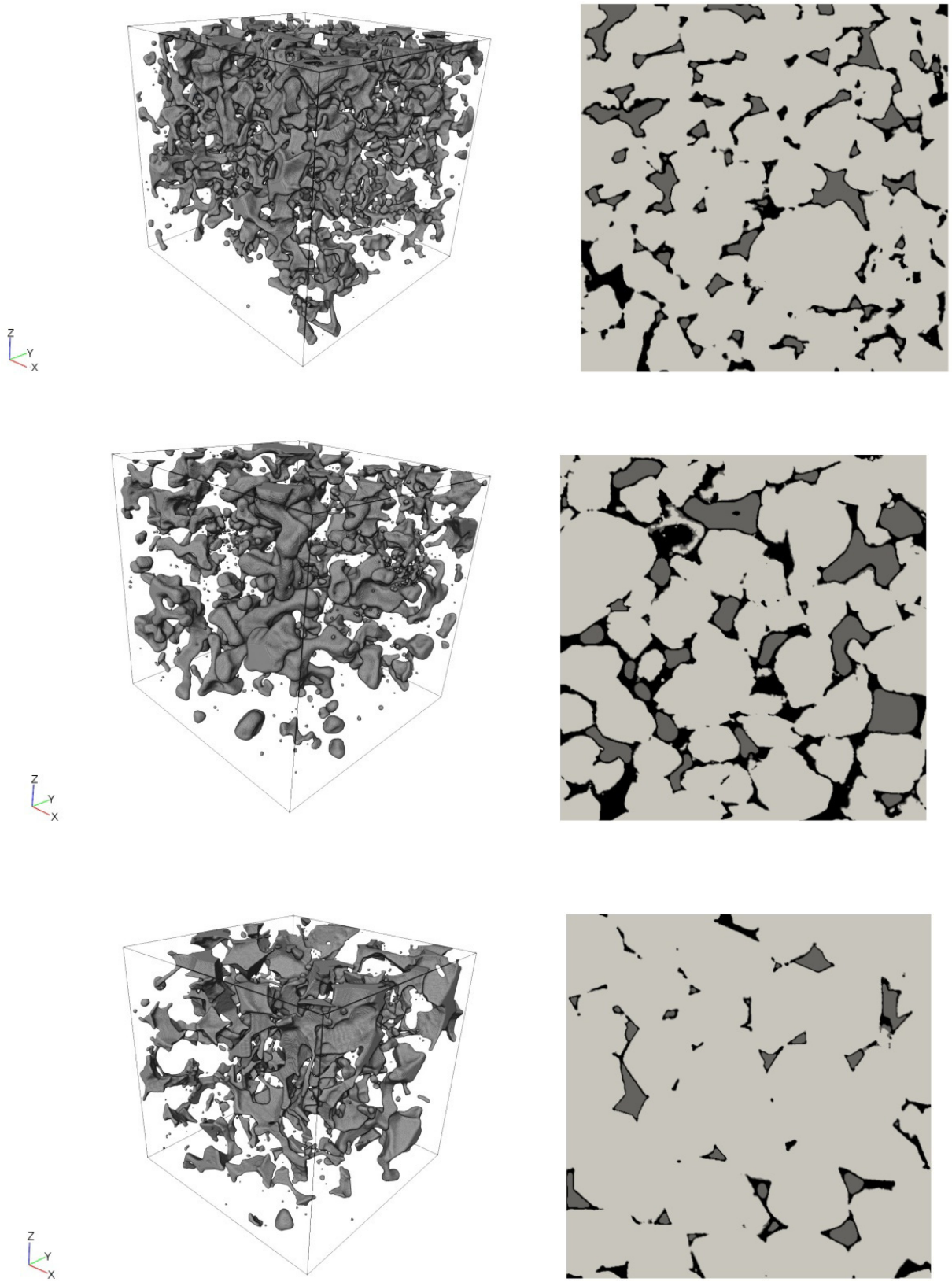

Fig. 4. 3D structures of residual oil and 2D slices of oil and water profiles after imbibition for Berea, Bentheimer and FB1 samples. In the 2D slices water is indicated by black, oil as dark gray and solid as light gray. In the 2D slices the z-axis is vertical and the y-axis points to the right.

Table 2. Comparison between simulation and experiment [1].

Rock Type		L (mm)	ϕ (%)	K_a (md)	FF	S_{oi} (%)	S_{or} (%)
Berea	Simulation	1.32	19.2	1221	19.8	78.6	42.5
	Experiment	75	19.4	208	19.0	78.9	48.2
		6	17.6				45.2
Bentheimer	Simulation	1.35	22.0	3048	14.0	90.5	35.8
	Experiment	72	22.1	2676	11.9	90.4	35.1
		6	23.1				45.2
Fontainebleau1	Simulation	1.03	11.4	270	50.5	91.1	52.5
	Experiment	80	14.1	304	48.7	90.4	25.0
		6	12.0				37.2

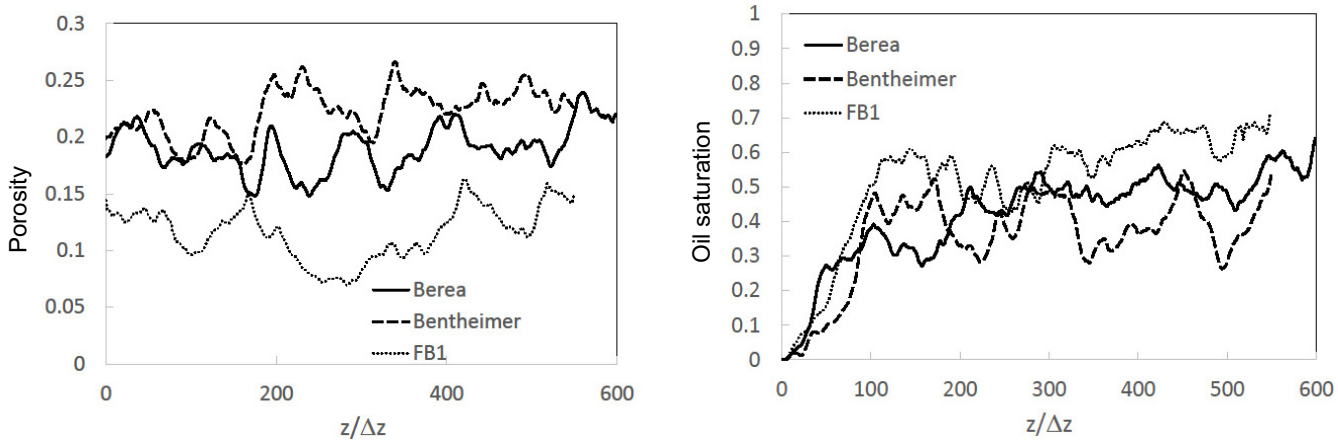

Fig. 5. Slice averaged porosity (left) profile and oil saturation profile after imbibition (right) for Berea, Bentheimer and Fontainebleau samples.

where the water enters the rock in the imbibition process. However, as further identified by the slice averaged oil saturation in Figure 5, the trapped oil is approximately uniformly distributed in the middle region that spans about 400 voxels. The uniformly distributed oil saturation indicates that the rock sample is large enough to be a representative volume for the imbibition process.

The pore size distribution of trapped oil cluster is compared to the pore body size distribution in the rock sample in Figure 6. The oil cluster size distribution is very close to the pore body size distribution and very slightly shifts to larger size. It indicates that oil is trapped in pores with different size of the rock sample. It is consistent with the oil clusters shown in Figure 4.

We investigated the dependence of residual oil saturation S_{or} on the initial oil saturation S_{oi} using the Berea sample. Figure 7 shows the applied capillary pressure as function of water saturation S_w for the Berea sample for different initial oil saturations $S_{oi} = 1 - S_w$. The residual oil saturation increases with initial oil saturation. The calculated oil saturation agrees well with experimental results as shown in Figure 8 [3]. In order to reduce the end effects (see Fig. 5) in the simulation the oil saturation was calculated by removing part of the sample that is located within 100 voxels from the both ends. The calculated data also agree well with the Land correlation, a widely used empirical model in literature [17]:

$$S_{or} = \frac{S_{oi}}{1 + S_{oi}\left(\frac{1}{S_{or}^{max}} - \frac{1}{1-S_{wc}}\right)} \quad (1)$$

Here S_{wc} is the connate wetting phase saturation. It has been assumed $S_{wc} = 0$ in the simulation. In Figure 9 the pore body and trapped oil cluster size distributions are plotted. The oil cluster size distribution gradually shifts to the larger size with decreasing initial oil saturation S_{oi}. For smaller initial oil saturation, the oil occupies the larger pore at beginning of the imbibition. Therefore the trapped oil occupied the larger pores after imbibition.

We simulated the drainage and imbibition process for eight Fontainebleau samples to investigate the effect of porosity. Figure 10 shows the applied capillary pressure as function of water saturation for different Fontainebleau samples. The dependence of residual oil saturation is plotted in Figure 11. The results of residual oil saturation are consistent with two sets of published experimental results in references [4, 5]. Fontainebleau is a mostly clay-free sandstone. The larger residual oil saturation at low porosity may result from larger pore body to throat size ratio. Aissaoui noticed that the pore throats sizes diminish with

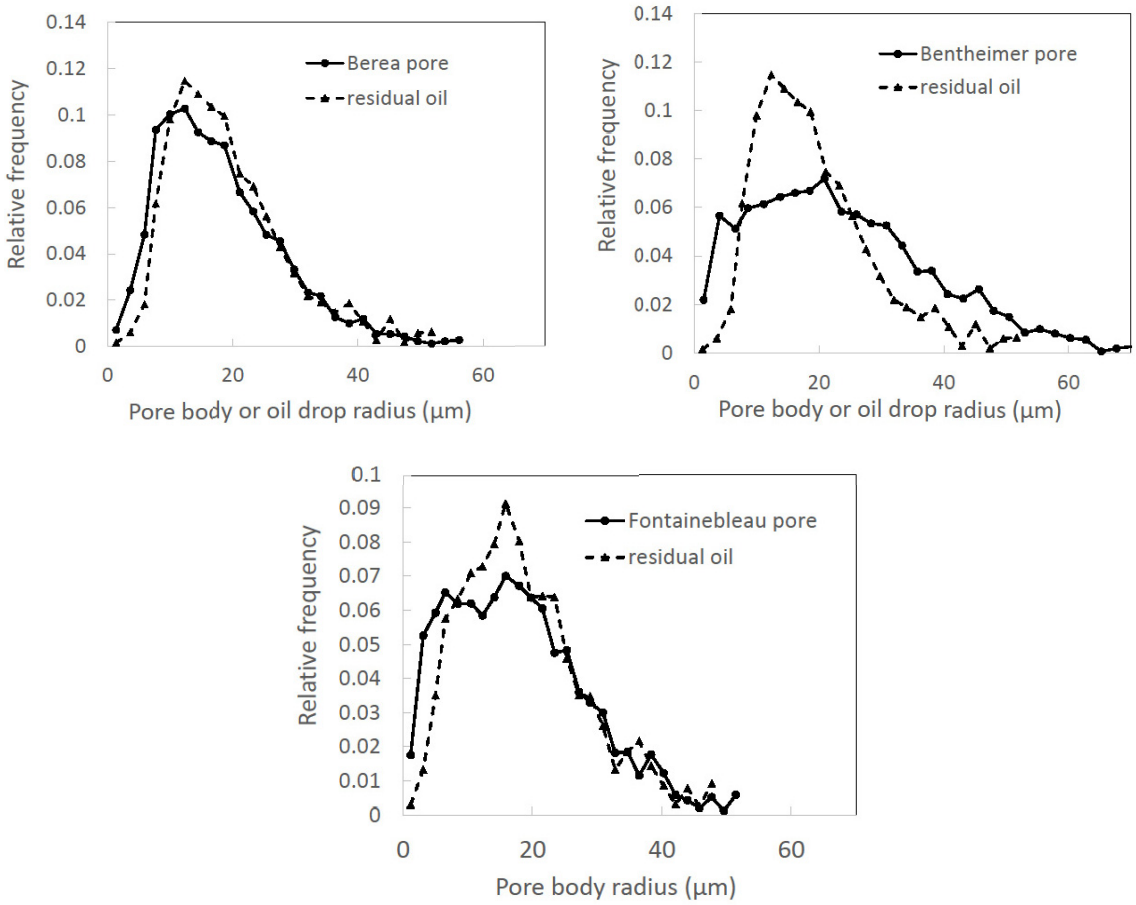

Fig. 6. Pore body and trapped oil drop radius distributions in the Berea, Bentheimer and Fontainebleau samples.

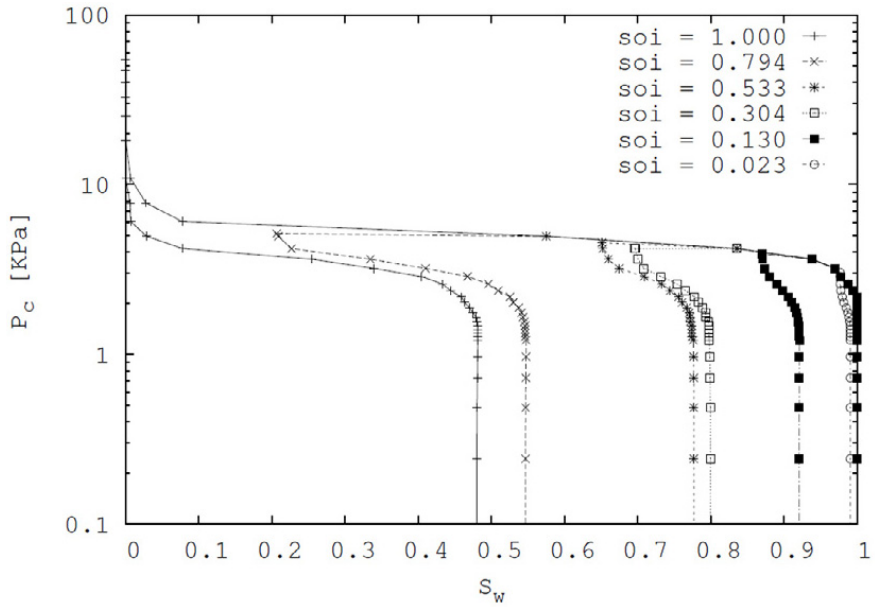

Fig. 7. Applied capillary pressure as function of water saturation S_w for the Berea sample for different initial oil saturations $S_{oi} = 1 - S_w$.

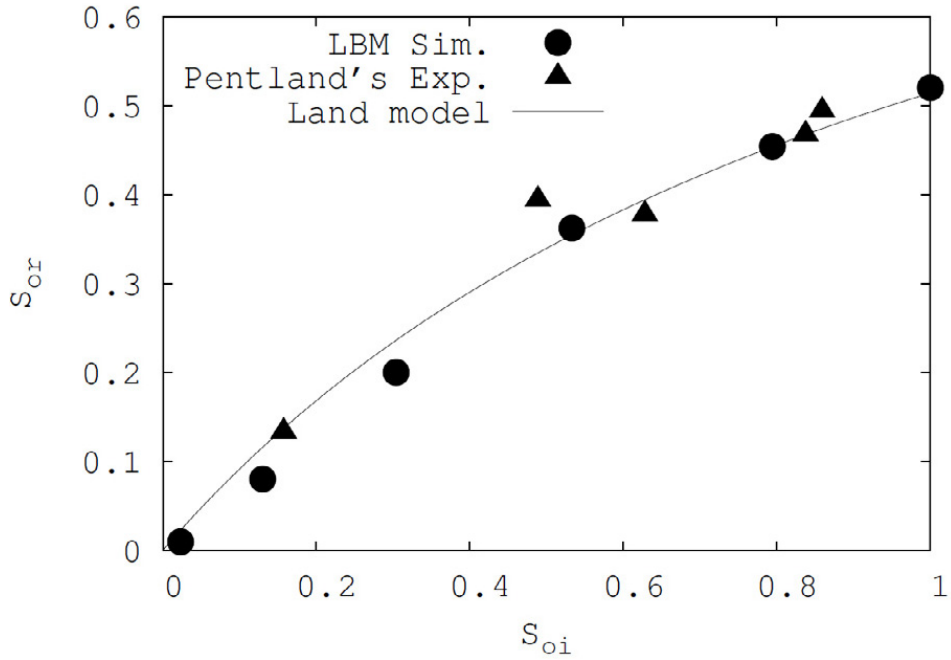

Fig. 8. Residual oil saturation as function of initial oil saturation for the Berea sample.

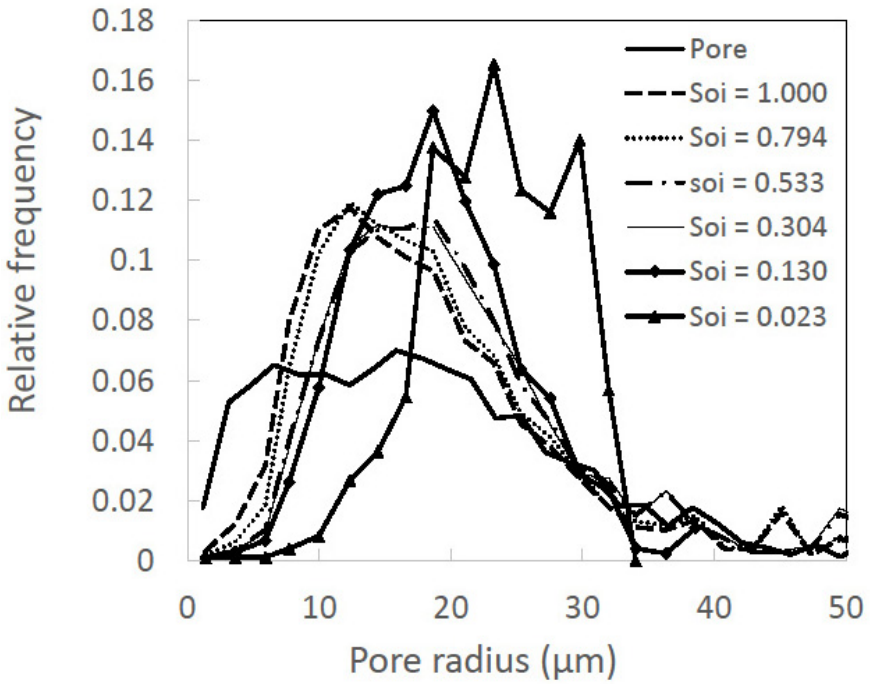

Fig. 9. Pore body and oil drop radius distributions after imbibition for different initial oil saturations S_{oi}.

porosity [18]. This is also true for our Fontainebleau rock samples evident in Figures 12 and 13. The pore body sizes for samples with different porosity are close while the pore throat size changes obviously with the porosity. Furthermore the pore body to throat size ratio was calculated. As shown in Figure 14, the pore body to throat size ratio and residual oil saturation S_{or} change with porosity in a similar manner. The correlation coefficients between S_{or} and R1 and between S_{or} and R2 are 0.94 and 0.93 respectively. Here two kinds of ratios are calculated by $R1 = \langle r_{pore}\rangle/\langle r_{throat}\rangle$ and $R2 = \langle r_{pore}/r_{throat}\rangle$. The brackets indicate an average.

Figure 15 shows pore body and trapped oil size distributions for the eight Fontainebleau samples. It is similar to what is observed in Figure 6 for the Berea, Bentheimer and FB1. The trapped oil cluster size distribution is close to the pore body size distribution of the rock sample and slightly shifts towards larger pore size. It indicates that

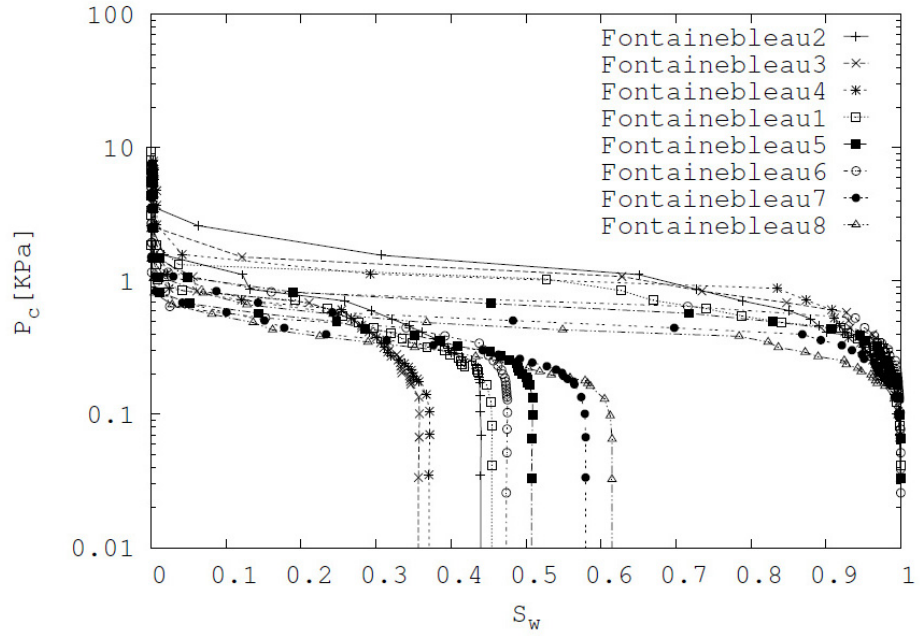

Fig. 10. Applied capillary pressure as function of water saturation for Fontainebleau samples.

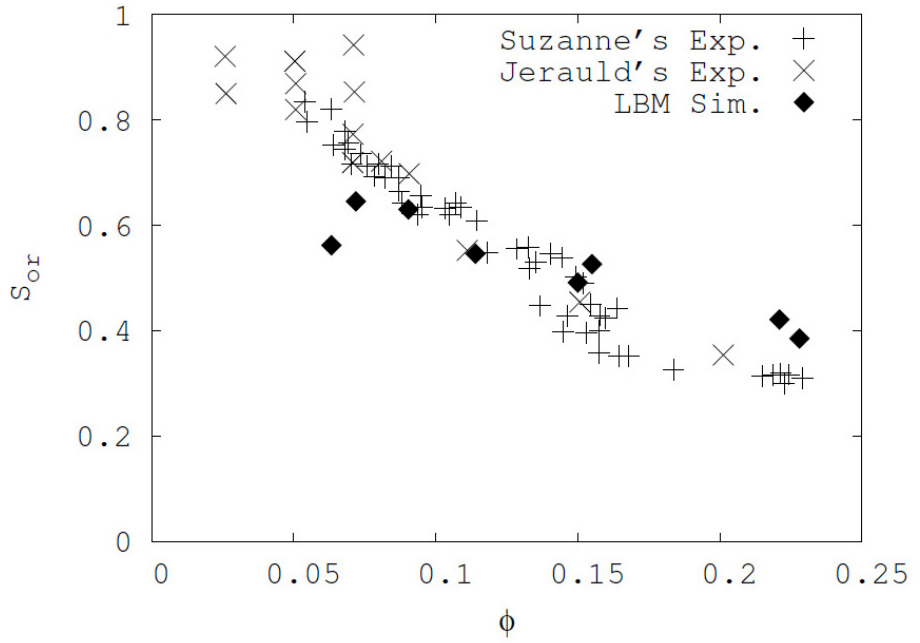

Fig. 11. Residual oil saturation as function of porosity for Fontainebleau samples.

oil is trapped in different sizes of pores and also is trapped in clusters of pores.

4 Conclusion

A lattice Boltzmann solver has been developed to investigate drainage and imbibition processes for different rock geometry, porosities and initial oil saturations in water wet conditions. The trapped oil after imbibition uniformly distributes in the middle of the sample. The oil is trapped in the center of pore bodies of different sizes while water stays in pore throats and on solid surfaces. The small oil clusters are sphere-like. The larger clusters occupies several pore bodies resembling the pore structure of the rock. The residual oil saturation and trapped oil cluster distributions after imbibition are consistent with recently reported experiments. The dependence of residual oil saturation on the initial oil saturation agrees well with the Land correlation. The residual oil saturation in Fontainebleau decreases with porosity and is highly correlated with the pore body to throat size ratio.

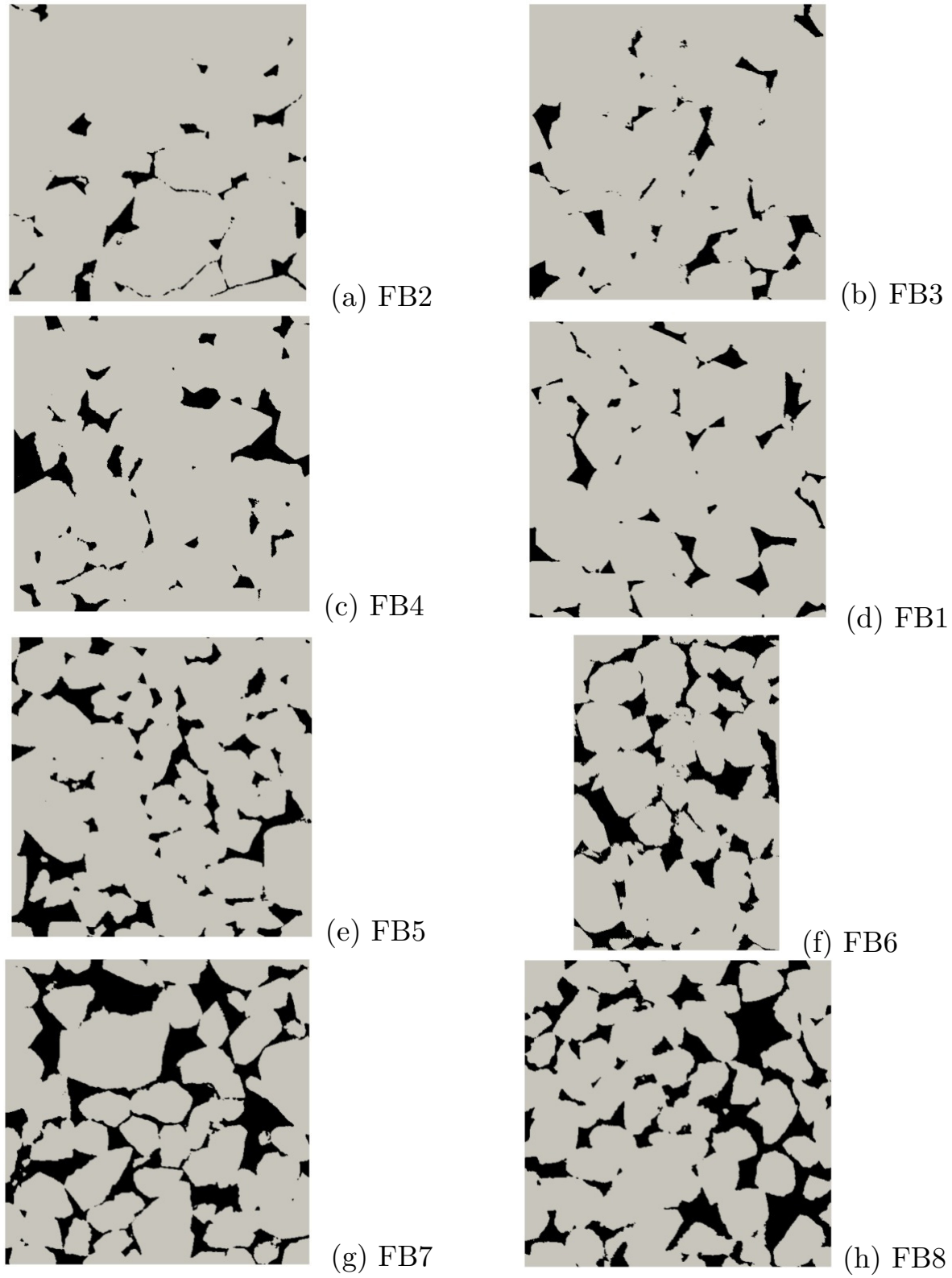

Fig. 12. 2D slices of Fontainebleau samples. The rock porosity increases from sample (a) to (h) gradually.

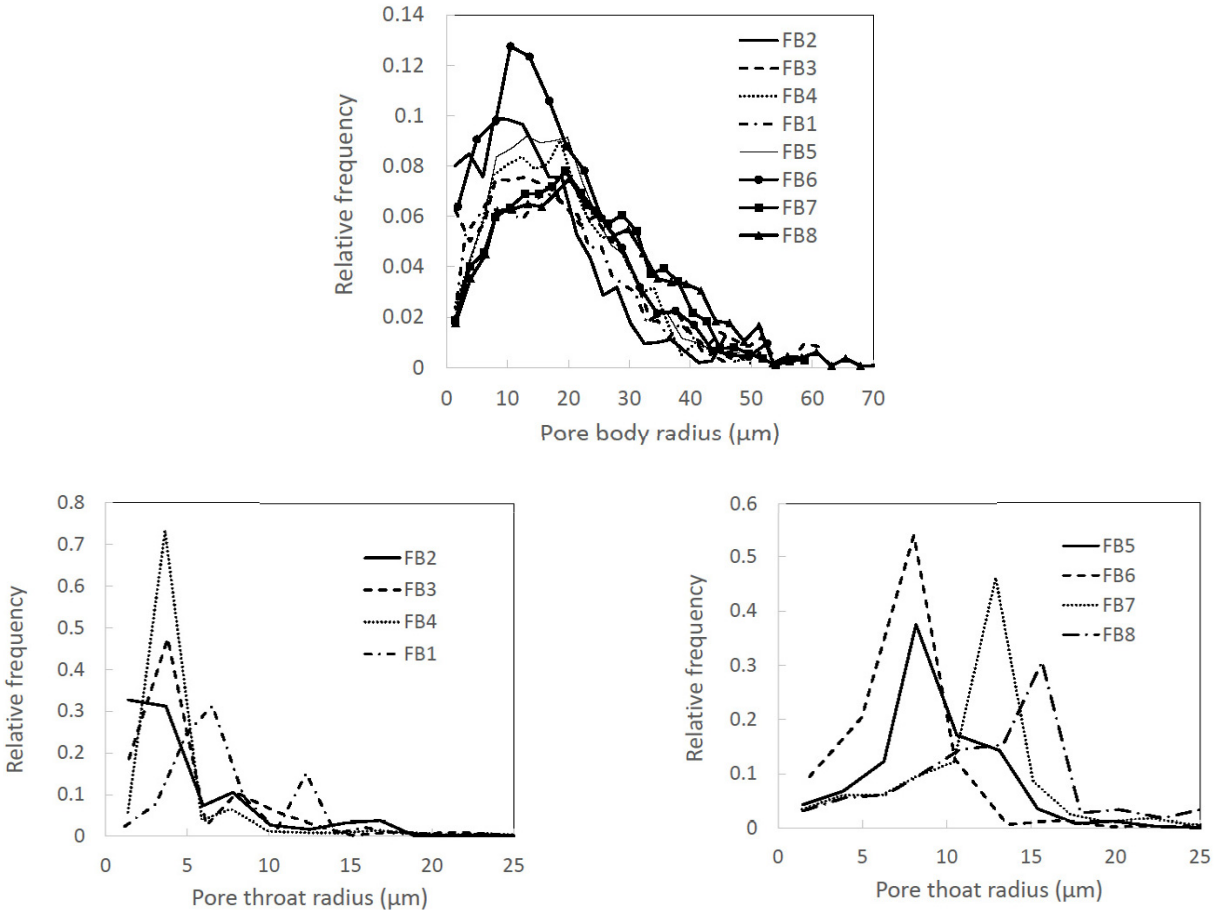

Fig. 13. Pore body (top) and pore throat radius distributions (bottom) for the eight Fontainebleau samples.

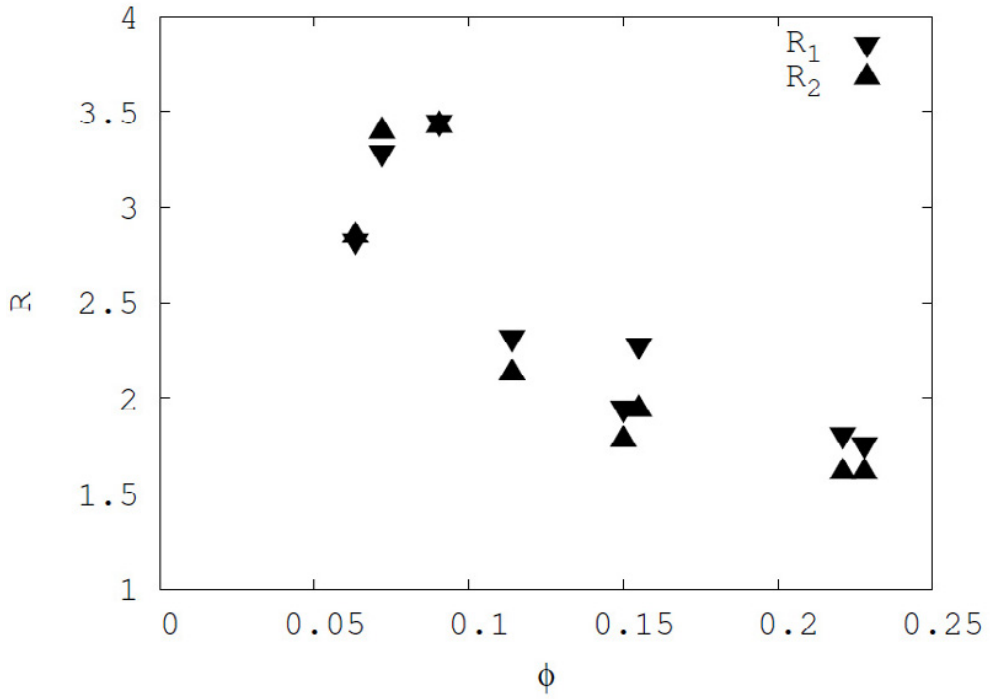

Fig. 14. Pore body to throat size ratio as function of porosity. Here $R1 = \langle r_{\rm pore}\rangle/\langle r_{\rm throat}\rangle$ and $R2 = \langle r_{\rm pore}/r_{\rm throat}\rangle$. The brackets indicate an average.

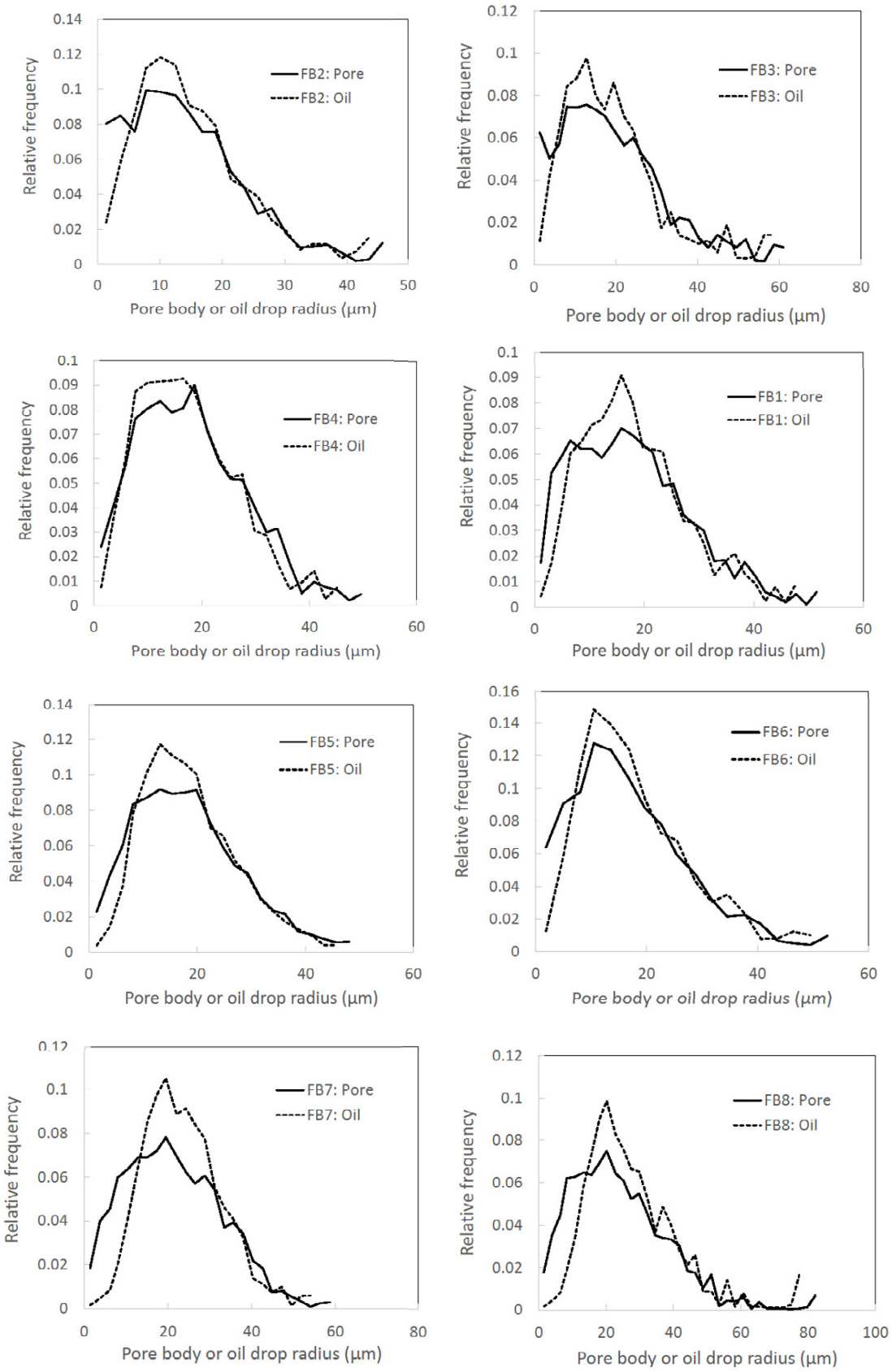

Fig. 15. Pore body and trapped oil radius distributions after imbibition for the eight Fontainebleau samples.

References

[1] R. Oughanem, S. Youssef, Y. Peysson, B. Bazin, E. Maire, O. Vizika, Pore-scale to core-scale study of capillary desatural curves using multi-scale 3D imaging, Proceedings of the Annual Symposium of the Society of Core Analysts, SCA 2013-027, Nap Valley, California, USA

[2] K.J. Humphry, B.M. Suijkerbuijk, H.A.J.M. van der Linde, S.G.J. Pieterse, S.K. Masalmeh, Impact of Wettability on Residual Oil Saturation and Capillary Desaturation Curves, Proceedings of the Annual Symposium of the Society of Core Analysts, SCA 2013-025, Nap Valley, California, USA

[3] C. Pentland, Y. Tanino, S. Iglauer, M. Blunt, Capillary Trapping in Water-Wet Sandstones: Coreflooding Experiments and Pore-Network Modeling. Paper SPE 133798 Proceedings of SPE Annual Technical Conference and Exhibition, Florence, Italy, 2010

[4] K. Suzanne, G. Hamon, J. Billiote, V. Trocme, Distribution of Trapped Gas Saturation in Heterogeneous Sandstone Reservoir, Proceedings of the Annual Symposium of the Society of Core Analysts, SCA2001-14, Edinburgh, Scotland, UK

[5] G.R. Jerauld, Gas-oil relative permeability of Prudhoe Bay, SPE 35718 presented at the western regional meeting held in Anchorage, Alaska, 1996, pp. 653–670

[6] E.J. Spiteri, R. Juanes, M.J. Blunt, F.M. Orr Jr., A New Model of Trapping and Relative Permeability Hysteresis for All Wettability Characteristics. SPE J. 13 (2008) 277–288.

[7] A. Al-Futaisi1, T.W. Patzek, Impact of wettability alteration on two-phase flow characteristics of sandstones: A quasi-static description, Water Resour. Res. 39 (2003) 1042–1051

[8] S. Chen, G.D. Doolen, Lattice Boltzmann method for fluid flows, Ann. Rev. Fluid Mech. 30 (1998) 329–64

[9] X. Nie, N.S. Martys, Breakdown of Chapman-Enskog expansion and the anisotropic effect for lattice-Boltzmann models of porous flow, Phys. Fluids 19 (2007) 011702–4

[10] I. Ginzburg, Consistent lattice Boltzmann schemes for the Brinkman model of porous flow and infinite Chapman-Enskog expansion, Phys. Rev. E 3 (2008) 0666704

[11] J. Tolke, X. Krafczyk, M. Schulz, E. Rank, Lattice Boltzmann simulations of binary fluid flow through porous media, Philos. Trans. R. Soc. London Ser. A 360 (2002) 535–545

[12] Y. Mu, Q. Fang, C. Baldwin, J. Toelke, A. Grader, M. Dernaika, Z. Kalam, Drainage and imbibition capillary pressure curves of carbonate reservoir rocks by digital rock physics. Proceedings of the Annual Symposium of the Society of Core Analysts, SCA 2012-056, Aberdeen, Scotland, UK

[13] H.J. Vogel, Morphological determination of pore connectivity as a function of pore size using serial sections, Eur. J. Soil Sci. 48 (1997) 365–377

[14] M. Hilpert, C.T. Miller, Pore-morphology-based simulation of drainage in totally wetting porous media, Adv. Water Resour. 24 (2001) 243–255

[15] D. D'Humieres, M. Bouzidi, P.T. Lalleman, Thirteen-velocity three-dimensional lattice Boltzmann model, Phys. Rev. E 63 (2001) 066702

[16] S. Iglauer, M.A. Ferno, P. Shearing, M.J. Blunt, Comparison of residual oil cluster size distribution, morphology and saturation in oil-wet and water-wet sandstone, J. Colloid Interface Sci. 375 (2012) 187–192

[17] C.S. Land, Calculation of imbibition relative permeability for two- and three-phase flow from rock properties, SPE J. 243 (1968) 149–156

[18] A. Aissaoui, Étude théorique et expérimentale de l'hystérésis des pressions capillaires et des perméabilités relatives en vue du stockage souterrain de gaz, Thesis École des Mines de Paris, 1983, 223 p.